Materials Research Letters

ISSN: (Print) 2166-3831 (Online) Journal homepage: https://www.tandfonline.com/loi/tmrl20

# Non-dissociated <c+a> dislocations in an AZ31 alloy revealed by transmission electron microscopy

Luoning Ma, Kelvin Xie, John Cai & Kevin J. Hemker

**To cite this article:** Luoning Ma, Kelvin Xie, John Cai & Kevin J. Hemker (2020) Non-dissociated <c+a> dislocations in an AZ31 alloy revealed by transmission electron microscopy, Materials Research Letters, 8:4, 145-150, DOI: 10.1080/21663831.2020.1721586

**To link to this article:** https://doi.org/10.1080/21663831.2020.1721586



Published online: 29 Jan 2020.

MATER. RES. LETT.
2020, VOL. 8, NO. 4, 145–150
https://doi.org/10.1080/21663831.2020.1721586

MATERIALS RESEARCH LETTERS
Taylor & Francis
Taylor & Francis Group

ORIGINAL REPORTS



# Non-dissociated <c+a> dislocations in an AZ31 alloy revealed by transmission electron microscopy

Luoning Ma [a], Kelvin Xie [b], John Cai [a] and Kevin J. Hemker [a]

[a]Department of Mechanical Engineering, Johns Hopkins University, Baltimore, MD, USA; [b]Department of Materials Science and Engineering, Texas A & M University, College Station, TX, USA

**ABSTRACT**

<c+a> dislocations in pure Mg have been reported to dissociate on basal planes, resulting in a sessile configuration that limits the ductility and formability of Mg. In this study, careful tilting experiments and weak-beam dark-field electron microscopy observations elucidated that <c+a> dislocations in the commercial alloy AZ31 remain compact without apparent dissociation. The stabilization of the <c+a> dislocation core structure with Al and Zn alloying may explain the improved strain to failure in the AZ31 alloy as compared to pure Mg samples.

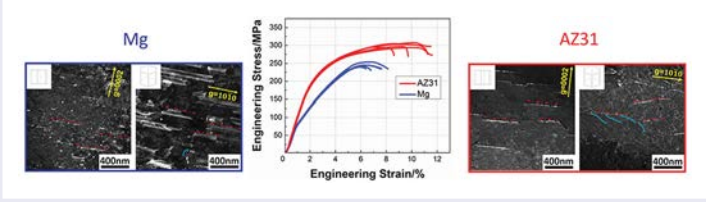


**IMPACT STATEMENT**

This paper involved detailed TEM analysis to elucidate an overlooked mechanism of non-dissociated <c+a> dislocations in AZ31 alloy that may contribute to improved ductility.

**ARTICLE HISTORY**
Received 2 September 2019

**KEYWORDS**
Magnesium; <c+a> dislocation; non-dissociation; ductility

## Introduction

With low density (23% that of steel and 66% that of aluminum) and high specific strength, Mg alloys are promising lightweight structural materials for energy efficient applications. However, wider usage of Mg is currently constrained by its limited room-temperature formability [1]. The low formability is correlated with the circumscribed pyramidal slip that contributes to compression along or tension perpendicular to the c-axis [2–4]. Improving the mobility of <c+a> dislocations is widely viewed to be a key to improving formability and unlocking expanded application of Mg.

To better understand the mechanism of <c+a> dislocation motion, c-axis compression experiments have been performed on Mg single crystals to activate non-basal pyramidal slip [4–6]. The motion of <c+a> dislocations on pyramidal planes (I and/or II) with Burger vectors along $<11\bar{2}\bar{3}>$ directions accommodate c-axis compression even though contraction twins [3] are occasionally observed at large deformation before failure [7]. TEM studies by Geng et al. [8] provided evidence to suggest that <c+a> dislocations in Mg are mostly 'basal bound' and non-conservatively dissociated into partial dislocations on the basal plane. The climb dissociation of <c+a> dislocations onto the basal plane has also been observed by Xie et al. [9] in their TEM study of Mg single crystals. These observations have been rationalized by Wu and Curtin [10] whose simulations indicate that the core of a <c+a> dislocation is metastable and undergoes either a thermally-activated transition to a sessile, basal-dissociated <c+a> or decomposition into a sessile <c> dislocation plus and a glissile <a> dislocation. Both dislocation core transformation mechanisms exhaust glissile <c+a> dislocations and result in low ductility. Stabilization of <c+a> dislocation cores to improve mobility has emerged as a promising strategy for improving the general ductility of Mg alloys, and it has been predicted that solid solution alloying may be an effective approach to stabilizing the <c+a> dislocation cores [10].

**CONTACT** Kevin J. Hemker hemker@jhu.edu 223 Latrobe Hall Room, Johns Hopkins University, 3400 North Charles Street, Baltimore, Maryland 21218, USA

Various studies were performed to investigate the effect of solid solution alloying on plasticity in Mg. Solution atoms, such as Y, Al and Li, have been shown to improve the ductility of Mg, which is deduced to be related to the improved activities of $<$c+a$>$ dislocations [4,11,12]. In parallel, simulations have associated the improved activity of $<$c+a$>$ dislocations with ductility. Sandlobes et al. [13] reported that decreased basal SFE results in easily formed stacking faults (SFs), which provide sources for $<$c+a$>$ dislocation nucleation. More recently, Wu et al. [14] investigated the correlation between cross-slip energy barriers of $<$c+a$>$ dislocations and ductility in a large number of potential solutes and predicted improved cross-slip with addition of rare earth elements, Mn, Ca and Zr, but their work did not provide definitive explanation for elements like Al or Zn. In the current study, to experimentally determine the influence of solutes (primarily Al and Zn) on the $<$c+a$>$ dislocation activity, we studied the commercial and widely available AZ31 [15] alloy as a model system to investigate $<$c+a$>$ dislocation behavior after close-to-c-axis compression and compare the findings with identical observations for pure Mg.

## Experiments

Hot-rolled pure Mg and AZ31 both have strong texture with the c-axis aligned along/close to the normal direction (ND). For both Mg and AZ31, rectangular compression samples with their longitudinal direction aligned along ND were electrical discharge machined (EDM) with dimensions of 3 mm × 3 mm × 6 mm. Pure Mg was annealed at 300°C for 3 h and AZ31 for 40 min due to the different grain sizes of as-rolled materials. The post annealed AZ31 and Mg have similar grain sizes and reduced dislocation densities. Quasi-static compression tests were conducted in an MTS machine at a strain rate of $10^{-4}$ $s^{-1}$ and the stress–strain curves were obtained for samples that were compressed to failure.

Electron backscatter diffraction (EBSD) was performed on the surface of as-annealed samples, and solute distribution was investigated using scanning transmission electron microscopy with an energy dispersive X-ray detector (STEM-EDX). Dislocation contrast was observed with weak-beam dark-field (WBDF) technique on a Tecnai 12 transmission electron microscope at 100 keV. TEM foils were cut from samples deformed to 2.5% strain and oriented with ND in plane of the foil. To avoid damage, both EBSD and TEM samples were mechanically polished under very low loads (nominally zero readings on the Allied automated polisher), and then electro-chemically polished with 10% nitric acid in methanol at −50°C.

## Results and discussion

The texture and grain size in both pure Mg and AZ31 were similar after the heat treatments described above. The average grain size of pure Mg ($65.1 \pm 27.3\ \mu$m) was comparable to that of AZ31 ($68.5 \pm 50.0\ \mu$m), as shown in Figure 1(c) and (f). Moreover, both types of samples exhibited similarly strong basal texture, see Figure 1(a,b). Thus, when investigating the mechanical properties, the effects of texture and grain size can be largely excluded. We note that the AZ31 samples possessed intrinsic precipitates and higher initial dislocation densities, even after annealing. In Mg, the pre-existing dislocations induced by hot-rolling were largely removed by the annealing [5] (see Figure 2). In AZ31, on the other hand, the dislocation density appears relatively high, likely because solute atoms and precipitates retard dislocation motion.

The distribution of solution atoms in the matrix and precipitates in AZ31 were mapped using STEM-EDX with corresponding maps of Mg, Al, Mn and Zn shown in Figure 2. All precipitates are rich in Al and Mn. The average diameter of precipitates after heat treatment is 28.3 nm which did not significantly increase compared to that before heat treatment (26.9 nm) [16]. The amount of Al and Zn in the matrix was measured to be 1.10 and 1.87 wt.%, respectively. The lower Al and higher Zn content in the matrix than the nominal composition of AZ31 (3 wt% Al and 1 wt.% Zn) can be ascribed to the formation of Al-rich precipitates and small errors in the measured compositions. In summary, Mg and AZ31 share similar texture and grain size after heat treatment, but the AZ31 alloy contains Al and Zn solute atoms in the matrix, a dispersion of nanoscale precipitates and residual dislocations.

The c-axis compression stress–strain curves of heat-treated pure Mg and AZ31 are shown in Figure 3. The ultimate compressive strength of AZ31 ($299.6 \pm 5.0$ MPa) is consistently higher than that of pure Mg ($243.2 \pm 7.4$ MPa). The average strain to failure of AZ31 ($9.87\% \pm 0.46\%$) is also consistently higher than that of pure Mg ($6.42\% \pm 0.27\%$) with a 49% increase. The higher ultimate compressive strength of AZ31 can be attributed to the interaction of dislocations with precipitates, pre-existing dislocations, and to a lesser extent, solute atoms. The improved strain to failure in the AZ31 samples was not expected and could be related to the fact that increased strain hardening inhibits plastic instabilities [17], but the affect that the solute atoms have on $<$c+a$>$ dislocation core geometry and the attendant mobility of $<$c+a$>$ dislocations must also be considered.

To unravel the effect of solid solution on $<$c+a$>$ dislocation behavior, the dislocations in pure Mg and

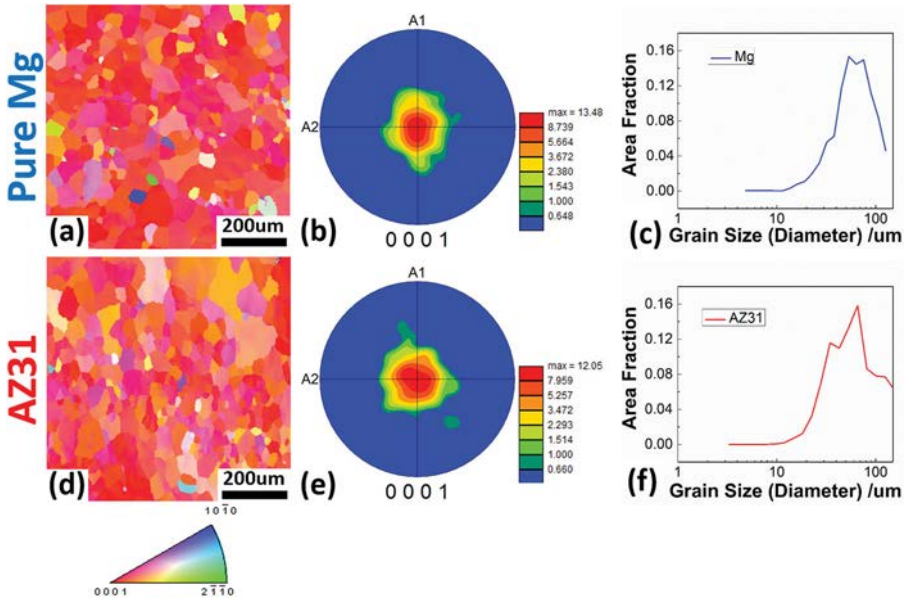


**Figure 1.** The microstructure of hot-rolled polycrystalline AZ31 and pure Mg after heat treatment with the normal of sample surface along ND. Inverse pole figures of (a) Mg and (d) AZ31 reveal strong basal texture after rolling. Pole figures of (b) Mg and (e) AZ31 with max values of 12 and 13.5, respectively, indicating that the textures are similar. Plots of the grain size distributions for (c) Mg and (f) AZ31 illustrates similar grain size for AZ31 ($d_{average} = 68.5\ \mu m$) and Mg (65.1 $\mu$m).

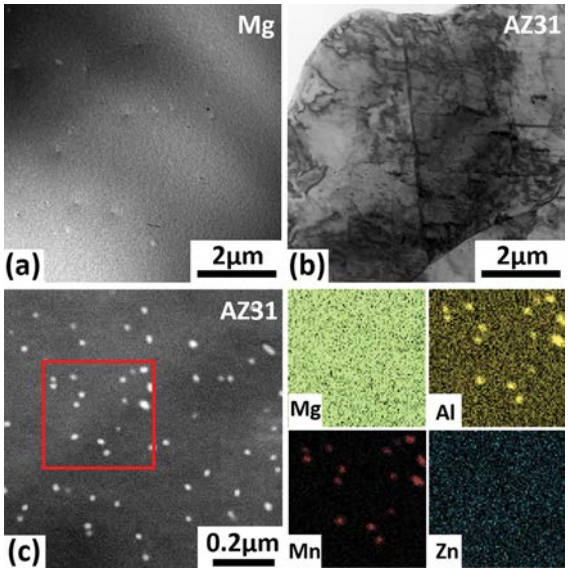


**Figure 2.** Bright-field TEM images of (a) pure Mg and (b) AZ31 after heat treatment obtained using one [11$\bar{2}$0] zone axis. (c) HADDF STEM image of a random area from AZ31 and the corresponding maps of Mg, Al, Mn and Zn (right) with respect to the area of interest marked as red box. These precipitates are rich in Al and Mn and the average diameter of precipitates in AZ31 is 28.34 nm.

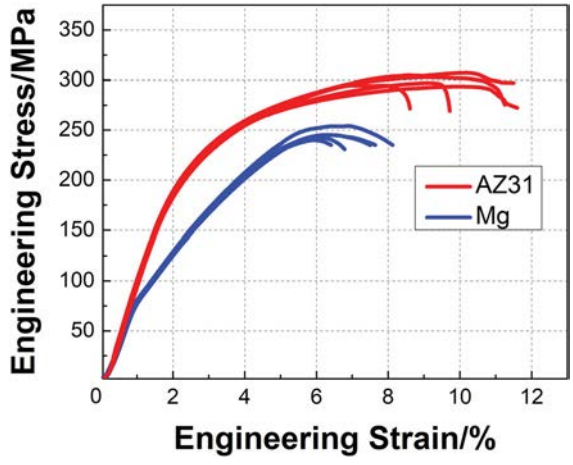


**Figure 3.** Engineering stress-strain curves of polycrystalline AZ31 Mg alloy (red) and pure Mg (blue) under compression along ND indicate consistently higher ultimate compressive strength and strain to failure of AZ31 than that of pure Mg.

AZ31 that were compressed by 3% under identical deformation conditions were imaged with WBDF at a series of tilt angles. One [11$\bar{2}$0] zone axis was selected and the $\mathbf{g}\cdot\mathbf{b} = 0$ invisibility criteria was utilized to deduce the Burgers vectors [4]. The diffraction vector $\mathbf{g}_c = [0002]$ was used to image $<c>$ dislocations ($\mathbf{b} = [0001]$) and the c-component in $<c+a>$ dislocations ($\mathbf{b}_{<c+a>} = 1/3[11\bar{2}\bar{3}]$), but $<a>$ dislocations ($\mathbf{b} = 1/3[11\bar{2}0]$) are invisible. By contrast, for $\mathbf{g}_a = [1\bar{1}00]$ diffraction vectors, $<a>$ dislocations and a-component in $<c+a>$ dislocations are visible but $<c>$ dislocations are invisible. Dislocations that are visible for both $\mathbf{g}_a$ and $\mathbf{g}_c$ are $<c+a>$ dislocations. Representative WBDF micrographs for pure Mg and AZ31 are given in Figure 4 with diffraction vectors illustrated

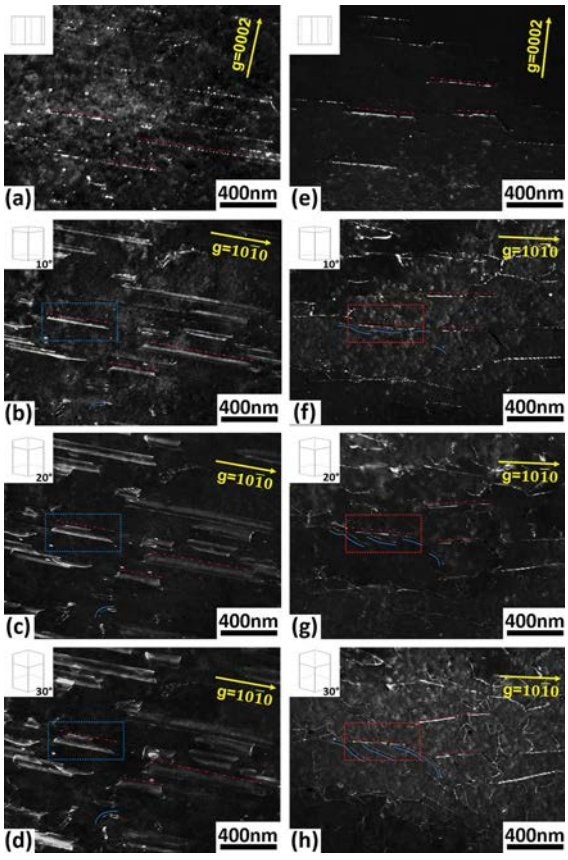


**Figure 4.** [Left Column]: WBDF images of pure Mg with: (a) the basal plane parallel to the incident beam with long straight intermittent lines lying parallel to the basal plane, and (b,c,d) the basal plane systematically tilted 10°, 20°, 30° from the electron beam revealing SF fringes. The widths of these faults indicate that they lie on the basal plane. [Right Column]: WBDF images of AZ31 taken with the same diffraction conditions. (e) Images taken with $\mathbf{g}_c = [0002]$ reveal long straight $<c+a>$ dislocations parallel to the basal plane, while (f,g,h) images taken at the same tilt angles as (b,c,d) indicate that the $<c+a>$ dislocations in AZ31 are compact with no evidence of SFs. For clarity, $<c+a>$ dislocations are marked with red dash lines and $<a>$ dislocations are marked with solid blue lines in all images. The pure $<a>$ dislocations are inclined in the thin foil and their periodic contrast is caused by thickness fringes; SFs were only observed for $<c+a>$ dislocations in pure Mg.

by yellow arrows. Examples of $<c+a>$ and pure $<a>$ dislocations are marked with red dash lines and solid blue lines respectively in all images.

Figure 4(a) is of pure Mg and was imaged using $\mathbf{g}_c = [0002]$; long straight intermittent thin white lines that appear to be $<c+a>$ dislocations can be observed lying parallel to the basal plane, which for this imaging condition is parallel to incident beam. By contrast, when the thin foil was tilted about $\mathbf{g}_a = [1\bar{1}00]$ and away from the $[11\bar{2}0]$ zone axis with the two-beam condition maintained (e.g. the $(1\bar{1}00)$ plane remains parallel to the incident electron beam but the basal plane is inclined at 10°, 20°, 30° from the electron beam), the $<c+a>$ dislocations that appeared to be long and straight in Figure 4(a) can now be seen to be dissociated on the basal plane with stacking fault (SF) fringes visible, similar to what was reported by Geng et al. [7] and Xie et al. [18].

The widths of SFs increase with tilting angle and scale with the projected area of the basal plane on the image plane, as shown in the top row of Figure 5. The nonconservative dissociation of $<c+a>$ dislocations creates a SF loop that is cut off by the free surfaces at the top and bottom of the TEM thin foil. A few curved dislocation segments can be seen in Figure 4(c,d), but most SFs only have partial dislocations visible at the ends. The long straight intermittent thin white lines in Figure 4(a) receive their contrast from the SF. When tilted, the thickness of each SF (t) follows a simple geometric relationship $t = T\sin\theta$, where T is the foil thickness (measured to be $181 \pm 15$ nm) and $\theta$ is the tilt angle (10°–30°), further confirming that the SF lies on basal plane. These basal dissociated $<c+a>$ dislocations indicate a core transformation from pyramidal to basal planes. After the transformation, $<c+a>$ dislocations transit from glissile to sessile and can no longer accommodate c-axis compression and can also retard the movement of glissle $<c+a>$ dislocations on the pyramidal plane. As a result, the mobility of $<c+a>$ dislocations and the attendant ductility of pure Mg is low.

Surprisingly, the $<c+a>$ dislocations that were observed in AZ31 displayed rather different behavior. The dislocations were imaged using the same diffraction vectors as for pure Mg and the WBDF images employing $\mathbf{g}_c = [0002]$ and $\mathbf{g}_a = [1\bar{1}00]$ are present in Figures 4(e–f) and 5. The $<c+a>$ dislocations in AZ31 were observed to align parallel to the basal plane and appeared compact when imaged with $\mathbf{g}_c = [0002]$, as shown in Figure 4(e). However, contrary to pure Mg, the $<c+a>$ dislocations in AZ31 remain compact with no apparent dissociation or fault fringes even when the basal plane is tilted by 30°, as shown in Figures 4(h) and 5. The compact nature of the $<c+a>$ dislocations in AZ31 provides strong experimental evidence that the dissociation energy is significantly increased by the addition of Al and Zn. With the more compact core structure, $<c+a>$ dislocations in AZ31 can be expected to be more mobile than the nonconservatively dissociated $<c+a>$ dislocations that are observed in pure Mg, and the increased mobility may be used to explain the higher strain to failure in the AZ31 samples. This correlation of alloying, dislocation core modification, and improved mechanical properties points to the role of $<c+a>$ dislocation cores in determining the mobility of $<c+a>$ dislocations and underpins a strategy for Mg alloy design: utilize solute atoms to suppress $<c+a>$ dislocation

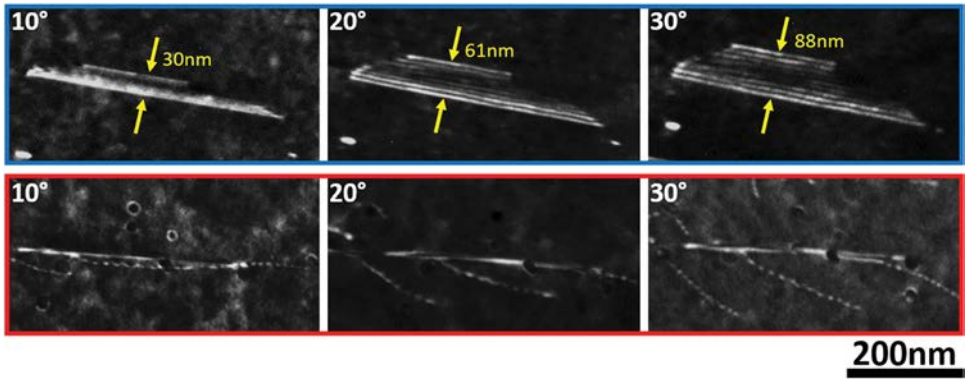


**Figure 5.** [TOP Row]: Magnified images of $<$c+a$>$ dislocation 1 of pure Mg taken in the area highlighted by blue dashed boxes in Figure 4(b–d); the thickness of the SF (t) follows t = Tsin$\theta$, where T is the foil thickness and $\theta$ is the tilt angle. [Bottom Row]: $<$c+a$>$ dislocation 1 of AZ31 taken in the area highlighted by red boxes in Figure 4(f–h); in contrast to pure Mg the AZ31 contains compact $<$c+a$>$ dislocations.

dissociations (ostensibly by increasing $<$c+a$>$ dissociation energy) and improve Mg alloy strain to failure and attendant formability. The magnitude of the effect is modest for AZ31, but extension to rare earth (RE) elements like Y, and potentially Ca, hold even greater promise.

It is worth noting that although AZ31 alloy displays improved strain to failure when compared to pure Mg, the amount of the improvement is modest (50%). One striking observation is that the $<$c+a$>$ dislocations in AZ31 are long and straight and aligned with the basal plane. This observation indicates that although these dislocations did not dissociate on the basal plane, the core might still relax into a nonplanar configuration. Determination of the dislocation line directions using the conventional projection approach indicates that the long straight $<$c+a$>$ dislocations numbered 1, 2 and 3 in Figure 4(a–d) are $[13\bar{3}\overline{10}\bar{3}]$, $[13\bar{3}\overline{10}\bar{3}]$ and $[12\bar{2}\overline{10}\bar{3}]$. Thus, $<$c+a$>$ dislocations in pure Mg are close to [10–10] and aligned along the intersection of the basal and pyramidal II planes. By contrast, individual dislocations in AZ31 were determined to have line directions of $[10\overline{2}\overline{1}\ 11\bar{3}]$, $[21\overline{1}\overline{1}\ \overline{10}\bar{5}]$ and $[5\bar{6}1\bar{1}]$. The first two are close to $<$1–210$>$ and associated with a pyramidal I plane, while the latter is close to $<$1–100$>$ and most closely associated with a pyramidal II plane. Within the experimental scatter associated with these measurements, these findings suggest that the origin of $<$c+a$>$ dislocations comes primarily from pyramidal II glide in pure Mg but that dislocation activity on both pyramidal planes is possible in AZ31. Wu et al. [14] discussed the competition between pyramidal-to-basal transition and pyramidal I-II cross-slip mechanisms and suggested that some elements, like Mn in AZ31, can decrease the average pyramidal I-II energy difference and enhance cross-slip and ductility. In this light, Al and Zn are not predicted to decrease the cross-slip barrier and the pyramidal-to-basal transition may still occur at the core level in AZ31 even though pyramidal I slip is available. Clearly more work and higher resolution observations of dislocation cores are needed.

## Summary and conclusions

In summary, $<$c+a$>$ dislocations were observed in both hot-rolled pure Mg and AZ31 after close-to-c-axis compression. The presence of Al and Zn in AZ31 was found to suppress the nonconservative dissociation of $<$c+a$>$ dislocations on the basal plane. This experimental finding parallels efforts in MD and DFT simulations and provides a benchmark for these efforts. The compact dislocation cores correlate to increased $<$c+a$>$ dislocation mobility and improved strain to failure for AZ31 as compared to pure Mg. The potential for using alloying to modify $<$c+a$>$ dislocation core geometries, in a way that has a transformative effect on $<$c+a$>$ dislocation mobility, and attendant ductility and formability, is expected to be even more potent in alloy systems (e.g. RE, Ca) that have been shown to have a positive influence in developing more formable Mg alloys.

## Acknowledgements

The authors would like to acknowledge the funding support from the National Science Foundation (NSF-DMR, grant number: 1709865, program manager: Gary Shiflet) for the financial support for this research.

## Disclosure statement

No potential conflict of interest was reported by the author(s).

## Funding

This work was supported by National Science Foundation [grant number 1709865].

## ORCID

*Luoning Ma* http://orcid.org/0000-0002-8869-3192

## References

[1] Mordike BL, Ebert T. Magnesium – properties – applications – potential. Mat Sci Eng A-Struct. 2001;302:37–45.
[2] Yoo MH, Morris JR, Ho KM, et al. Nonbasal deformation modes of HCP metals and alloys: role of dislocation source and mobility. Metall Mater Trans A. 2002;33:813–822.
[3] Xie KY, Alam Z, Caffee A, et al. Pyramidal I slip in c-axis compressed Mg single crystals. Scripta Mater. 2016;112:75–78.
[4] Agnew SR, Horton JA, Yoo MH. Transmission electron microscopy investigation of < c+a > dislocations in Mg and alpha-solid solution Mg-Li alloys. Metall Mater Trans A. 2002;33:851–858.
[5] Obara T, Yoshinga H, Morozumi S. [112bar2](11bar23) slip system in magnesium. Acta Metall Mater. 1973;21:845–853.
[6] Syed B, Geng J, Mishra RK, et al. [0001] compression response at room temperature of single-crystal magnesium. Scripta Mater. 2012;67:700–703.
[7] Geng J, Chisholm MF, Mishra RK, et al. The structure of < c+a > type dislocation loops in magnesium. Philos Mag Lett. 2014;94:377–386.
[8] Geng J, Chisholm MF, Mishra RK, et al. An electron microscopy study of dislocation structures in Mg single crystals compressed along [0001] at room temperature. Philos Mag. 2015;95:3910–3932.
[9] Xie KY, Reddy KM, Ma L, et al. Experimental observations of the mechanisms associated with the high hardening and low strain to failure of magnesium. Materialia. 2019;8: 100504.
[10] Wu ZX, Curtin WA. The origins of high hardening and low ductility in magnesium. Nature. 2015;526:62–67.
[11] Sandlobes S, Friak M, Neugebauer J, et al. Basal and nonbasal dislocation slip in Mg-Y. Mat Sci Eng A-Struct. 2013;576:61–68.
[12] Sandlobes S, Friak M, Zaefferer S, et al. The relation between ductility and stacking fault energies in Mg and Mg-Y alloys. Acta Mater. 2012;60:3011–3021.
[13] Sandlobes S, Pei Z, Friak M, et al. Ductility improvement of Mg alloys by solid solution: Ab initio modeling, synthesis and mechanical properties. Acta Mater. 2014;70:92–104.
[14] Wu Z, Ahmad R, Yin B, et al. Mechanistic origin and prediction of enhanced ductility in magnesium alloys. Science. 2018;359:447–452.
[15] Bhattacharyya JJ, Agnew SR, Muralidharan G. Texture enhancement during grain growth of magnesium alloy AZ31B. Acta Mater. 2015;86:80–94.
[16] Dogan E, Wang S, Vaughan MW, et al. Dynamic precipitation in Mg-3Al-1Zn alloy during different plastic deformation modes. Acta Mater. 2016;116:1–13.
[17] Zhu Y, Wu X. Ductility and plasticity of nanostructured metals: differences and issues. Mater Today Nano. 2018;2:15–20.
[18] Xie K, Reddy KM, Ma L, et al. Experimental observations of the mechanisms associated with the high hardening and low strain to failure of magnesium. Materialia. 2019;8:100504.